Optical study of extended-molecular-layer flat islands in lattice-matched $In_{0.53}Ga_{0.47}As/InP$ and $In_{0.53}Ga_{0.47}As/In_{1-x}Ga_xAs_yP_{1-y}$ quantum wells grown by low-pressure metal-organic vapor-phase epitaxy with different interruption cycles

R. Sauer,* S. Nilsson,† P. Roentgen, W. Heuberger, and V. Graf
IBM Research Laboratory, Säumerstrasse 4, CH-8803 Rüschlikon/Zürich, Switzerland

A. Hangleiter
4. Physikalisches Institut, Universität Stuttgart, Pfaffenwaldring 57, D-7000 Stuttgart 80, Federal Republic of Germany

R. Spycher
Institut de Microscopie Electronique, Ecole Polytechnique Fédérale, CH-1015 Lausanne, Switzerland
(Received 9 March 1992)

Growth of lattice-matched $In_{0.53}Ga_{0.47}As/InP$ and $In_{0.53}Ga_{0.47}As/In_{1-x}Ga_xAs_yP_{1-y}$ quantum wells (QW's) by low-pressure metal-organic vapor-phase epitaxy with specific growth-interruption cycles leads to three simultaneous effects in the photoluminescence (PL) spectra: (I) energy shifts of all PL lines, (II) line broadenings, and (III) splitting of individual QW lines into multiplets associated with the formation of extended molecular-layer (ML) flat islands. Samples were grown with four or six single QW's exhibiting overlapping PL multiplets with up to twelve "coherent" lines in sequence and ML thickness differences of their parent islands. It is shown, by temperature-controlled PL and PL-decay-time measurements, that these flat islands behave as independent QW's at low temperatures, thus giving evidence of their large extensions. The unambiguous assignments of PL energies to island widths made possible by the coherence of the line sequence demonstrate significant and systematic deviations from pertinent theoretical calculations based on square-well potentials. It is argued that the potentials are not ideally squarelike but rather graded in the well due to an initial excess indium concentration caused by switching perturbations of the gas fluxes. For $In_{0.53}Ga_{0.47}As/In_{1-x}Ga_xAs_yP_{1-y}$ QW's this extra potential (i.e., the band-gap variation of $In_{1-x}Ga_xAs$) is estimated to be ≈ 30 meV with a relaxation length of order 100 Å along the growth direction. The corresponding excess indium concentration is $\approx 6\%$ over the lattice-match composition of 53%. Scanning cathodoluminescence (CL) was employed taking CL images and spot excitation spectra. "Monochromatic" images, recorded with light detection at different wavelengths of a particular luminescence line, reveal complementary, complex-shaped dark-bright lateral regions. The complementary regions fit perfectly together, even in details down to lateral extensions of below 1 μm. We conclude that such structure originates from lateral fluctuations of the nonsquare QW potentials associated with the composition gradient in the growth-interruption cycle.

I. INTRODUCTION

In the past few years the effect of growth interruption on the optical properties of quantum wells (QW's) has been studied to some extent for samples grown by molecular-beam epitaxy (MBE) and metal-organic vapor-phase epitaxy (MOVPE) both in GaAs-based material systems[1–12] and in InP-based systems,[13–15] and in $In_{0.53}Ga_{0.47}As/In_{0.52}Al_{0.48}As$.[16] Observed is, either in low-temperature photoluminescence (PL) or absorption, the splitting of the $n=1$ QW transitions into multiplets due to the formation of extended flat islands within a given quantum well differing in width L_z by single molecular layers (ML's). As a standard model it is assumed that growth interruption allows additional surface migration to smooth out residual roughness of the heterointerfaces. However, line splittings associated with atomically abrupt extended QW islands were also observed (although sometimes less distinct) when the crystal growth was not interrupted but with growth conditions "optimized."[17–20] Figures of merit in this respect are crystal growth on substrates which are exactly oriented parallel to (001) planes (whereas 2° misorientation, e.g., leads to single, unsplit QW lines), or low growth temperatures to make timing as precise as possible and to minimize transition effects. This was recently demonstrated in MOVPE grown $In_{1-x}Ga_xAs_yP_{1-y}/InP$ QW's by Thijs and co-workers[21,22] and in $In_{1-x}Ga_xAs/InP$ QW's grown by vapor levitation epitaxy by Morais *et al.*,[23] respectively. In both cases, significant splitting effects were observed without growth interruption.

In the present paper, we investigate a variety of lattice-matched $In_{0.53}Ga_{0.47}As/InP$ and $In_{0.53}Ga_{0.47}As/In_{1-x}Ga_xAs_yP_{1-y}$ ($y \approx 2.2x$) quantum wells grown by low-pressure MOVPE as a function of substrate orientation and different growth interruption cycles. We study in detail such samples where the splitting of QW PL lines into multiplets is particularly pronounced and leads to "enumerable" sequences of transitions, namely, up to 12 overlapping peaks from four nom-

inal QW's in a particular sample. Transmission electron micrographs confirm the presence of four QW's and allow the determination of their average widths. We ascribe the appearance of the PL multiplets to the formation of extended flat islands with constant thicknesses L_z over the island regions, equal to multiple numbers of molecular layers, $a_0/2=2.9347$ Å, in the following also referred to as monolayers.[24] Such samples are ideal for systematic physical studies since no uncontrollable sample-to-sample growth fluctuations emerge. The coherence of the PL line sequence removes the uncertainty in determining island widths L_z, and allows us to study L_z-dependent effects, such as confinement energies, on a firm quantitative basis. We study the optical properties of the monolayer islands by photoluminescence, photoluminescence excitation (PLE), temperature-controlled PL, and luminescence-decay-time measurements, and scanning cathodoluminescence (SCL) recording spectrally resolved cathodoluminescence (CL) images and fixed-spot-excitation spectra.

II. EXPERIMENT

$In_{0.53}Ga_{0.47}As/InP$ and $In_{0.53}Ga_{0.47}As/In_{1-x}Ga_xAs_yP_{1-y}$ heterostructures were grown by low-pressure metal-organic vapor-phase epitaxy (LPMOVPE) at 630 °C, 100 mbar in a horizontal, lamp-heated reactor at a typical growth rate of 9–12 Å/sec. Trimethylindium (TMIn), trimethylgallium (TMGa), 100% PH_3, and AsH_3 were used as gas sources. Gas flow and switching was controlled by a computer with an accuracy in time of 0.1 sec. Lattice matching of the $In_{0.53}Ga_{0.47}As$ and $In_{1-x}Ga_xAs_yP_{1-y}$ layers with respect to the Fe-doped InP substrates is better than $|\Delta a/a|<1\times10^{-3}$ as confirmed by double-crystal x-ray diffraction.

PL spectra were taken at sample temperatures from ≈2 to 300 K in various optical cryostats. The samples were either immersed in liquid helium or cooled in a helium vapor stream at a controlled temperature. The spectra were excited by red (Kr) or green (Ar) laser lines or by filtered incandescent lamp light, dispersed by different grating monochromators up to 1 m focal length, detected by cooled Ge detectors and processed by conventional lock-in techniques. Time-resolved spectra taken at sample temperatures from 1.7 to 4.2 K were excited by a cavity-dumped mode-locked Ar laser (514-nm line, single pulse duration ≈150 psec, repetition frequency ≈800 kHz) and low average power $P\approx0.5$ mW to avoid sample heating. They were detected by a cooled $S1$-cathode photomultiplier (time resolution $\Delta t\approx0.3$ nsec) or a Ge avalanche photodiode ($\Delta t\approx0.6$ nsec) employing time correlated photon counting.

Scanning cathodoluminescence was performed with a scanning electron microscope (International Scientific Instruments/Akashi Seisakusho, ISI-DS-130) equipped with a LaB_6 filament source and an adapted cold stage (Oxford Instruments) enabling sample temperatures of ≈6 K. The diameter of the electron beam hitting the sample surface is ≈40 Å. However, the spatial resolution of the CL system corresponds to the "recombination volume" of excess electrons and holes which is much larger. It is given by the generation volume and carrier diffusion out of this volume. For an acceleration voltage of 4 kV used in our experiments the electron penetration depth is ≈0.3 μm (Ref. 25) which we take as a measure for the generation volume. Lateral transport investigations by optical time-of-flight measurements indicate that in the lattice-matched $In_{0.53}Ga_{0.47}As/InP$ system for QW's with $L_z\approx10$ Å the (ambipolar) diffusion length is of order 2 μm at cryogenic temperatures;[26] this value can be much smaller at significant impurity or defect concentrations. Hence, a spatial resolution of ≈2 μm or better was assumed in the CL experiments.

Transmission electron microscopy (TEM) studies were performed on cleaved wedges in a Philips EM430 ST electron microscope with a point-to-point resolution of 2 Å. 90° wedges parallel to [001] were obtained by cleavage along two perpendicular ⟨110⟩ directions and were investigated along the [100] direction. Both standard TEM bright field and high-resolution TEM were performed. Details of the method are given in Refs. 27–29. The wedge observation technique avoids any artifact due to sample preparation (ion milling, etc.) and is very powerful for chemical analysis.[29,30] Bright field imaging in the microscope yields equal thickness fringes as the electron intensity in the transmitted beam is oscillating with the thickness. The fringes run in parallel with the edge in the case of a wedge-shaped sample. The distance between these oscillations is sensitive to the composition of the crystal thus enabling composition analysis down to approximately 5% accuracy.

III. SUBSTRATE MISORIENTATION AND GROWTH INTERRUPTION CYCLES: EFFECTS ON PHOTOLUMINESCENCE SPECTRA

Many samples of lattice-matched $In_{0.53}Ga_{0.47}As/InP$ quantum wells and $In_{0.53}Ga_{0.47}As/In_{1-x}Ga_xAs_yP_{1-y}$ ($\lambda=1.1$ and 1.3 μm) quantum wells were grown and characterized routinely by low-temperature PL. They differ in their substrate (mis)orientations and growth-interruption cycles. The substrates are (001) type and either exactly oriented with an accuracy of $\pm0.2°$ or misoriented 2° off the (001) plane towards [110]. Growth interruption includes three times: t_1, t_2, and t_3. For the barrier material InP, for instance, growth was interrupted with the group-III element In. The flux of the group-V component P exceeded that of In for a time t_1. The As flux was then started with a delay time t_2 after interrupting the P flux. The group-III components in the QW, In, and Ga, were added after an additional time t_3. At the heterointerface between QW and barrier, the same sequence of interruption times was applied in the reverse order of the components. A schematic sketch of the interruption cycle is shown in Fig. 1. In a preliminary stage of the growth experiments all three interruption times were varied. It was found that variation of t_1 and t_2 had no significant effect on the optical properties of the QW's as long as $t_1<10$ sec and $t_2<2$ sec. The term "optical property" is meant to include PL intensity, linewidth, and variation of line positions. Hence, standard values were used in the following: $t_1=1$ sec and

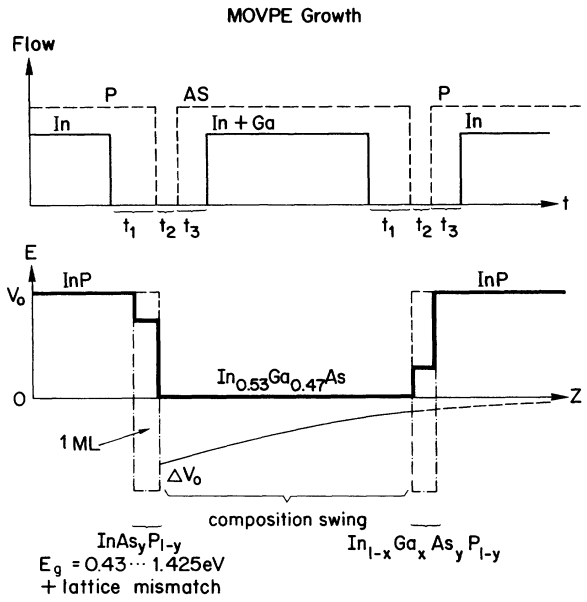

FIG. 1. Top: Flow diagram in the LP MOVPE growth for $In_{0.53}Ga_{0.47}As/InP$ quantum wells defining the interruption times t_1, t_2, and t_3. Bottom: Possible associated quantum-well potentials for electrons. Three models are shown: square-well potential with abrupt interfaces (dashed line), square-well potential with an additional alloy step 1-ML wide (broad solid line or dashed-dotted line), and potential with composition swing $\Delta V(z)$ in the $In_{0.53}Ga_{0.47}As$ QW (narrow solid line).

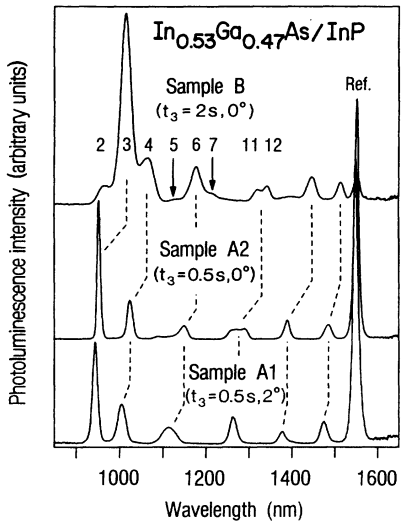

FIG. 2. Photoluminescence spectra ($T \approx 10$ K) of three $In_{0.53}Ga_{0.47}As/InP$ quantum-well samples. Included in parentheses are the growth-interruption times t_3 and substrate misorientations off (001) for samples A_1, A_2, and B. All samples incorporate six QW's. For sample B the PL lines split into multiplets which partially overlap. Line numbers refer to island widths in molecular layers (ML's). Identification of the lines was performed as described in detail in the text for sample C (Fig. 3).

$t_2 = 0$ or 0.5 sec. (See Table I.) Variation of t_3 from 0 to 10 sec influenced the PL spectra depending on the substrate orientation. This is demonstrated in Fig. 2 for three samples of $In_{0.53}Ga_{0.47}As/InP$. Samples grown on exactly oriented substrates exhibit, in a systematic way, three simultaneous effects with increasing t_3: (I) The lines split into multiplets, (II) they broaden significantly, and (III) the centers of the multiplets shift to lower energies. There is also a reduction in intensity of the reference layer peak for low optical excitation in such samples, but no appreciable intensities of impurity bands are observed. As shown in Fig. 2, the reference layer ($\approx$2000-Å wide) virtually does not change emission wavelength, and concomitant x-ray-diffraction studies performed on each sample did not show significant changes in composition. Therefore, we conclude that these effects are not due to the introduction of mismatch strain. To study the effect of substrate misorientation, constant interruption times of $t_3 = 0.5$ sec were chosen. Growth on substrates misoriented by 2° off (001) generally led to broad linewidths for all QW lines of a sample and to shifts toward higher photon energies compared to simultaneous growth on oriented substrates (Fig. 2). This result is consistent with findings of other groups in MOVPE and MBE growth.[21,22]

Basically the same effects were observed for $In_{0.53}Ga_{0.47}As/In_{1-x}Ga_xAs_yP_{1-y}$. The splitting effect was even stronger in the $In_{0.53}Ga_{0.47}As/In_{1-x}Ga_xAs_yP_{1-y}$ system. This is shown in Fig. 3 for two samples (C and D) each incorporating a stack of four QW's grown with $t_3 = 2$ sec. The QW growth times were 20, 10, 5, and 2 sec (sample C) and 20, 10, 3, and 1 sec (sample D). To remove uncertainties in the determination of the QW widths from growth times alone, sample

TABLE I. Substrate orientation and t_3 growth-interruption time of the samples $A1$, $A2$, B, C, and D.

Sample	Material system	Substrate orientation	Group-V preflow time t_3
$A1$	$In_{0.53}Ga_{0.47}As/InP$	(001), 2° off towards [110]	0.5
$A2$	$In_{0.53}Ga_{0.47}As/InP$	(001)±0.2°	0.5
B	$In_{0.53}Ga_{0.47}As/InP$	(001)±0.2°	2.0
C	$In_{0.53}Ga_{0.47}As/In_{1-x}Ga_xAs_yP_{1-y}$	(001)±0.2°	2.0
D	$In_{0.53}Ga_{0.47}As/In_{1-x}Ga_xAs_yP_{1-y}$	(001)±0.2°	2.0

C was investigated by transmission electron microscopy (Fig. 4). The high-resolution image (Fig. 4, top) yields the width of the widest QW to be (94±3) Å. The widths of the other QW's observed in bright field were related to this value and found to be 42, 28, and ≈12 Å, with a reference layer of $L_z = 1450$ Å. The thickness fringes in Fig. 4 are parallel to the edge ending abruptly at the well-barrier interfaces. This indicates good composition homogeneity in the barriers. In the PL spectrum of sample C (Fig. 3, bottom) the four QW's give rise to the lines between 1150 and 1500 nm. They are arranged in four corresponding groups which we assign as the 1.47-μm line ($L_z = 94$ Å), group centered at 1.42 μm ($L_z = 42$ Å), group centered at 1.33 μm ($L_z = 28$ Å), and group centered at ≈1.22 μm ($L_z = 12$ Å). The two latter multiplets overlap, possibly with contributions to the line labeled 6 from both of the wells with $L_z = 28$ Å and ≈12 Å. PL spectra at $T = 4.2$ K instead of 2 K (as in Fig. 3) show a distinct shoulder on the high-energy side of the peak labeled 14. The residual peaks at the lowest and highest energies in the spectrum are associated with the bulklike thick reference layer and with the barrier, respectively. Comparison with literature data[31] yields the composition of the $In_{1-x}Ga_xAs_yP_{1-y}$ barrier to be $y \approx 0.42$ ($x \approx 0.19$).

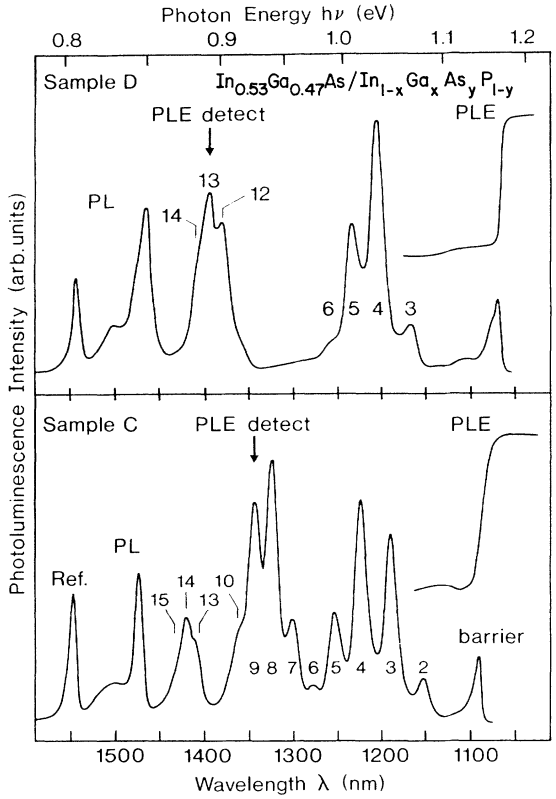

FIG. 3. Photoluminescence spectra ($T = 2$ K) of two lattice-matched $In_{0.53}Ga_{0.47}As/In_{1-x}Ga_xAs_yP_{1-y}$ ($\lambda = 1.1$ μm) quantum-well samples. Plotted are also photoluminescence excitation (PLE) spectra, with indication of the detection wavelength, showing the band-edge absorption of the barrier material. This yields $y \approx 0.42$, $x \approx 0.19$ for sample C and $y \approx 0.38$, $x \approx 0.17$ for sample D. Each sample incorporates an ≈1500-Å-thick $In_{0.53}Ga_{0.47}As$ reference layer and four QW's, with growth times of 20, 10, 3, and 1 sec (sample D) and 20, 10, 5, and 2 sec (sample C). Line numbers refer to the widths L_z of the parent flat islands in integral numbers of molecular layers (1 ML = 2.935 Å). They were determined as discussed in the text.

Similar to sample C a multiplet structure is observed for sample D (Fig. 3) which contains also four QW's. The assignment of the 1.47-μm and the 1.39-μm line groups to the two thickest QW's is unambiguous. Comparison to sample C suggests that the group centered at ≈1.22 μm is preferentially due to the second narrowest QW. It is unclear whether the narrowest QW grown for only 1 sec is optically active and contributes part of the intensity of the latter multiplet. The undulations between 1.1 and 1.15 μm could originate from this QW. The position of the barrier peak yields a slightly different composition of $In_{1-x}Ga_xAs_yP_{1-y}$ in this sample, $y \approx 0.39$ ($x \approx 0.18$), while x-ray-diffraction measurements show lattice matching of barrier and well material. This composition change explains why peaks in the spectrum of sample D fall to valley positions for sample C and vice versa at high energies.

In both samples, positions and spacings of the multiplet lines correspond very closely to QW's that differ in width L_z by a single monolayer, 1 ML = 2.935 Å (cf. below for details). Hence, we interpret the multiplet splitting as being due to the formation of extended ML-flat islands within a QW differing in width by $\Delta L_z = 1$ ML. It is important to note that the perfect energetic coincidence of the multiplet lines from different QW's and the very systematic energetic sequence of all observed lines (cf. also Fig. 8) demonstrates the existence of islands with *accurately defined* widths L_z. The line labels chosen in Fig. 3 refer to the number of monolayers of the emitting QW island. Arguments for our particular assignment are given in Sec. V below. At 2 K, the PL spectra of samples C and D do not change under excitation with red or green laser lines or with narrow-band-excitation light from an incandescent lamp. The relative intensities of the lines also do not change when the excitation of a red laser (Kr: 647.1 nm) is varied from a few microwatts to milliwatts. The insensitivity of the spectrum to excitation intensities in a very wide range is a measure for the high sample quality since otherwise, for low excitation, wavelength shifts and relative intensity changes are often observed for QW PL lines. Photoluminescence excitation measurements, performed with a lamp-monochromator combination to excite the PL, showed no sharp structure with detection on any of the PL lines but a steep edge at around 1.1 μm due to band-edge absorption in the barrier (Fig. 3). The onset of the edge coincides with the highest PL energy peak and shows that this peak is due to emission from the $In_{1-x}Ga_xAs_yP_{1-y}$ barrier material. The small energy spacing between these peaks in the independently grown samples C and D is a measure for the good composition control in our MOVPE growth. In the following section, we study in detail sample C of Fig. 3.

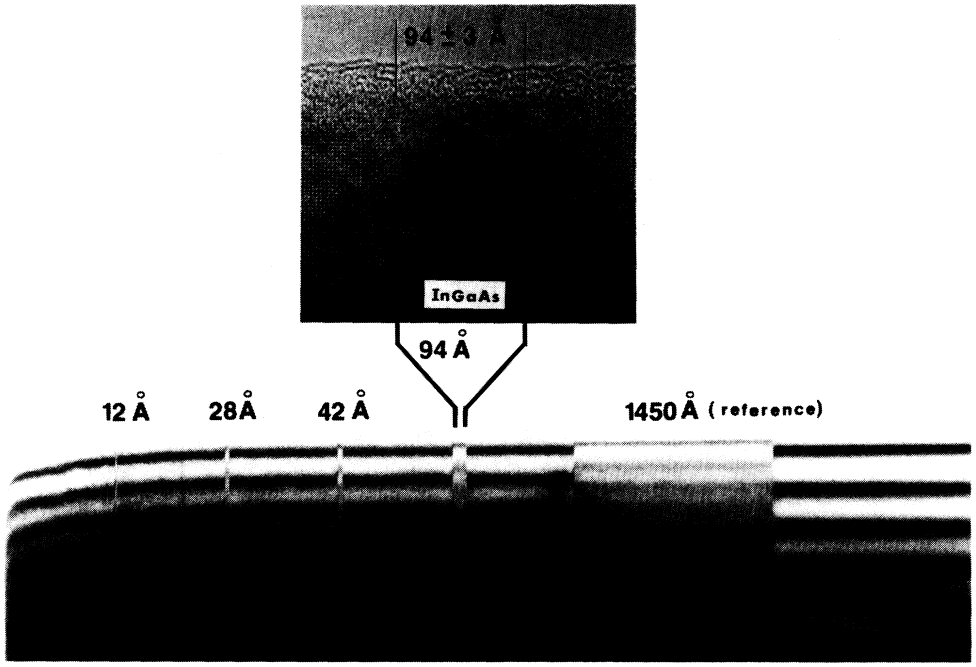

FIG. 4. Transmission electron microscopic picture of part of sample C ($In_{0.53}Ga_{0.47}As/In_{0.81}Ga_{0.19}As_{0.42}P_{0.58}$) showing the four QW's and the reference layer. The high-resolution picture on top yields the thickness of the widest QW, $L_z=(94\pm3)$ Å, and is used to calibrate the bright field image on the bottom. The widths obtained for the three remaining QW's are $L_z=42$, 28, and ≈ 12 Å. The reference layer of $In_{0.53}Ga_{0.47}As$ is 1450-Å thick.

IV. ML ISLANDS: TEMPERATURE-CONTROLLED PL AND LUMINESCENCE DECAY MEASUREMENTS

Temperature-dependent PL spectra of sample C are shown in Fig. 5. The appearance of multiplet lines with nonthermal intensity distributions from up to five different ML islands in one QW demonstrates that the islands are decoupled at low temperatures. Up to 90 K, the integral intensities from the two thinnest wells are comparable and, relatively, do not change much. In contrast, there is a significant, and very similar, redistribution of multiplet line intensities within the two QW groups: In both groups, higher temperatures favor the emission of lower energetic multiplet lines. This effect is ascribed to enhanced diffusion of electrons and holes at higher temperatures: excess carriers created in one ML island reach adjacent islands within their lifetime. In the range of 90 K, the available thermal energies of $kT\approx 7.5$ meV are not sufficient to significantly populate higher energetic states so that quasithermalization to islands with lower energetic states is obtained. In a similar way, but at lower temperatures of 20 K, Zachau and Grützmacher[32] observed diffusion of excitons to low-energy QW islands in $In_{1-x}Ga_xAs/InP$ in absorption. The present higher temperatures needed for interdiffusion could indicate that the island sizes are larger or the mobilities poorer in our samples than in this work. The situation is different for the *integral* intensities of the QW's. For temperatures higher than 90 K essentially all PL from the thinnest well is quenched, due to dissociation of the electrons and holes into the barrier.

Time-resolved PL measurements confirm the view of decoupled ML islands at low temperatures. The measurements were performed on a total of 19 lines of samples C and D. The lines, in a spectral range from 1.1 to 1.55 μm, were all measured using a fast Ge avalanche diode. The higher-energy lines, between 1.115 and 1.25 μm, were strong enough to be studied in addition with a $S1$-cathode-type photomultiplier. The results were identical. A typical luminescence decay curve as observed for the stronger peaks is shown in Fig. 6. The decay of the 4-ML peak in Fig. 6 is purely exponential over more than two orders of magnitude. The decay time does not change for excitation strengths increased by a factor of order 10. It also does not change at 4.2 K. The time-resolved measurements are summarized in Fig. 7. The error bars depicted for the peaks close to 40-Å QW width are not due to the scattering of the individual sampling points on a given curve; instead they reflect the fact that the decay curves are no longer exponential but superpositions of at least two exponentials. This hints to the participation of additional recombination channels, e.g., via donor or acceptor related states, but was not further investigated in the present paper. The experimental points in Fig. 7, closed squares or open circles, represent the dominant exponential portion of the decay. Some of these points around $L_z=40$ Å appear a little high within the sequence of decay times; however, on the whole it is clear that these lifetimes form a characteristic curve with high values for narrow wells, a strong decrease towards broader wells, a minimum at $L_z\approx 30$ Å, and finally a reincrease of the lifetimes for broad wells. These trends are

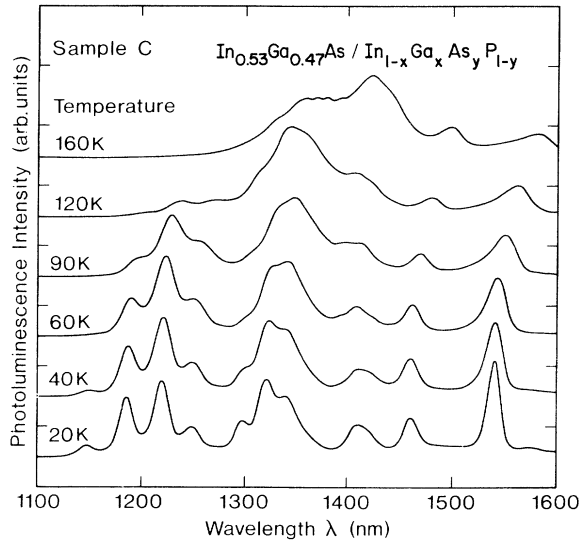

FIG. 5. Photoluminescence spectra of sample *C* ($In_{0.53}Ga_{0.47}As/In_{0.81}Ga_{0.19}As_{0.42}P_{0.58}$) at different temperatures.

reminiscent—though much more distinctive here—of recent decay time measurements on a six-QW stack of lattice-matched $In_{0.53}Ga_{0.47}As/InP$ grown by chemical-beam epitaxy (CBE).[33,34] In the latter case, an interpretation of the experimental results was successfully based on 2D exciton dynamics as adopted from theoretical considerations[35] under certain plausible simplifications; these concerned weak dependences on L_z of some of the parameters involved, or partial cancellations of the L_z dependences of such parameters. Since the material system $In_{0.53}Ga_{0.47}As/InP$ studied there is much related to the present $In_{0.53}Ga_{0.47}As/In_{1-x}Ga_xAs_yP_{1-y}$ system, we apply in the present work the same simplifications as made by Cebulla and co-workers[33,34] and, for brevity, cite only the original and final expressions for the 2D-exciton

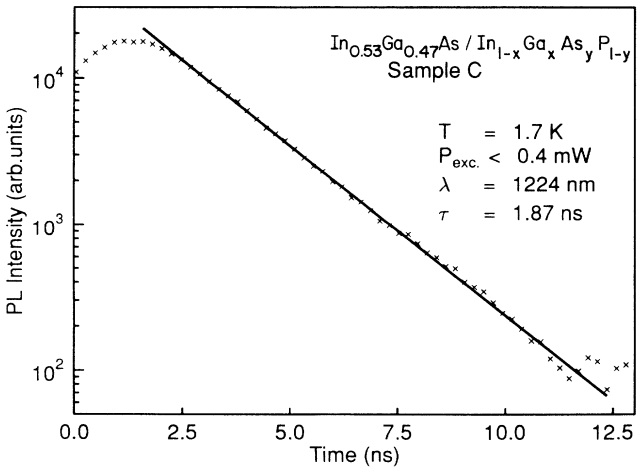

FIG. 6. Photoluminescence decay curve at $T=1.7$ K of the 4-ML peak of sample *C* (cf. Fig. 3). The least-squares fit (full line) corresponds to a decay time $\tau=1.87$ nsec.

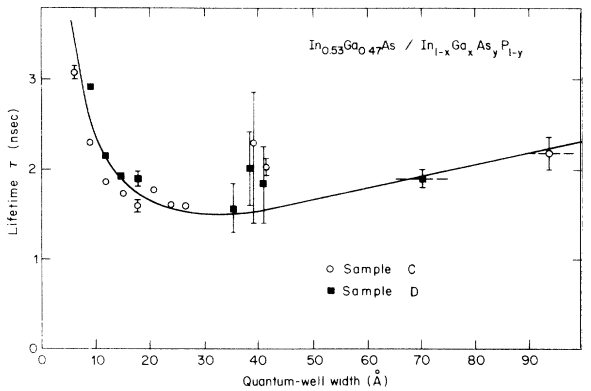

FIG. 7. Luminescence decay times vs relevant quantum-well widths (= island widths) at low temperature, $T=1.7$ or 4.2 K. Circles: sample *C*; squares: sample *D*. Full line, theoretical model as described in the text. PL line assignments to QW widths are as in Fig. 3 (see text).

lifetimes as discussed previously. The original expression for the transition strength of the 2D free excitons is[35]

$$F_x^{2D}=f_0[4\pi h^2 r(T)][A_x\Delta(T)M]^{-1}, \tag{1}$$

where f_0 is the oscillator strength, $r(T)$ the fraction of excitons contributing to the recombination, A_x the area of the 2D excitons for a 2D Bohr radius $a_0(L_z)$, $\Delta(T)$ the homogeneous linewidth of the excitons, and M the sum of electron and heavy-hole masses $m_e^*+m_{hh}^*$.[36] This expression was transformed, using applicable simplifications as mentioned, into an expression for the exciton lifetime τ proportional to $(F_x^{2D})^{-1}$,

$$\tau=\text{const}\times\langle z\rangle\langle\rho^2\rangle\frac{1}{f_0}, \tag{2}$$

where $\langle z\rangle$ is the average extension of the exciton in the growth direction z and $\langle\rho^2\rangle$ is the average extension of the exciton in the area perpendicular to z. The L_z dependence of the latter parameter was neglected and the residual parameters were expressed in terms of the envelope wave functions Ψ_e and Ψ_h of the confined electrons and heavy holes, respectively.[33] The oscillator strength is proportional to the electron-hole overlap $f_0\propto|\int\Psi_e\Psi_h dz|^2$ and $\langle z\rangle$ was taken as the geometrical average of the halfwidths Δz_{FWHM} of the squared envelope wave functions:[33]

$$\langle z\rangle\propto\{[\Delta z_{FWHM}(\Psi_e)]^2[\Delta z_{FWHM}(\Psi_h)]^2\}^{1/2}. \tag{3}$$

This procedure finally allows us to express τ as a function of $\Psi_e(L_z)$ and $\Psi_h(L_z)$, all other parameters being only proportionality factors. In the present work we have calculated τ as a function of L_z in a square-well potential model using Bastard's boundary conditions[37] at the heterointerfaces, and normalizing the functions accordingly in the whole z range, $-\infty\le z\le+\infty$. The result is shown in Fig. 7 as the full line. Only a constant factor was employed as an adjustable parameter shifting the model curve up or down as a whole for optimum coincidence with the measured lifetimes. The agreement is

good including the very narrow wells $L_z < 20$ Å where the lifetime measurements of Cebulla and co-workers[33,34] did not yield a convincing trend towards higher τ values. Therefore, the present data are the first to establish definitively a lifetime minimum for quantum wells of thickness $L_z \approx 20-30$ Å. We note that the lifetimes measured by Engel *et al.*[38] in MOVPE grown $In_{1-x}Ga_xAs/InP$ quantum wells significantly decrease from $L_z = 200$ Å down to ≈ 15 Å but do not show a minimum. There is a significant scatter in their data possibly since they were taken from several independently grown samples. Also, lifetime values for QW's of the same nominal width but different origin are widely spread: for $L_z \approx 20$ Å, Cebulla and co-workers[33,34] find approximately 0.8 ns ($T = 2$ K), Engel *et al.*[38] $\approx 4-6$ ns ($T = 7$ K), and our value in Fig. 7 is around 1.6 ns ($T = 2$ K). The large difference between the low- and high-temperature data could be sought in long-lived temperature activated feedback channels for the exciton population, such as donor-acceptor pairs, although this was not discussed by Engel *et al.*[38]

The agreement of our data with the theoretical model developed for independent single QW's are a direct manifestation that each ML-flat island in our samples can be considered as an isolated QW with no "communication" (i.e., diffusion and, optically, apparent thermalization) with its neighboring islands at low temperatures. Within a given QW this is only possible when the island size is larger, on the average, than the exciton diffusion length plus exciton diameter. In this case, the multiplet line intensities should reflect the relative size distribution of the ML islands within a QW. In fact, envelopes on the PL multiplets from sample *C* yield average QW widths of ≈ 14 ML $= 41.1$ Å, ≈ 8.3 ML $= 24.4$ Å, and ≈ 3.8 ML $= 11.2$ Å, consistent with the corresponding TEM values.

V. CONFINEMENT ENERGIES AND QW POTENTIAL

The peak wavelengths in the PL spectrum of sample *C* at 2 K are listed in Table II. The energy upshifts from the $In_{0.53}Ga_{0.47}As$ wide layer reference peak at 801 meV (1.547 μm) are plotted in Fig. 8 as a function of the QW island widths L_z. It is apparent that the peaks represent a coherent sequence of energies given by ML width differences of their parent islands. There are no missing members up to the region around 1.39 μm (Fig. 3) or $\simeq 100$-meV upshift (Fig. 8), respectively. The eye guideline in Fig. 8 shows that in this spectral region two peaks are missing. Given the absolutely smooth empirical curve through all data points we can exclude that one or three peaks are missing. In either case, the guideline would have a kink with slopes from both sides that would not fit together. It follows that we are concerned with a sequence of totally 14 coherent data points.

The data points significantly disagree with theoretical confinement energies in square-well potentials for *any absolute assignment* of PL lines to QW widths L_z. This is essentially due to the "wrong" shape of the theoretical curve which is too flat compared to the data points. The discrepancies cannot be reconciled by small variations of the parameters used in Fig. 8 to calculate the square-well potential curve. Also, these parameters are firmly established; this holds for the total band offset which is directly observed in our case, the offset partitioning between electrons and holes, and the band-edge masses. Energy-dependent masses due to the coupling of electrons, light holes, and split-off holes shift up the square-well potential curve, thus increasing the discrepancies. Details are discussed in Appendix A also including the influence of the exciton binding energy. It is important to note that the inconsistency between experimental and theoretical curves is not sample specific but general since it is ob-

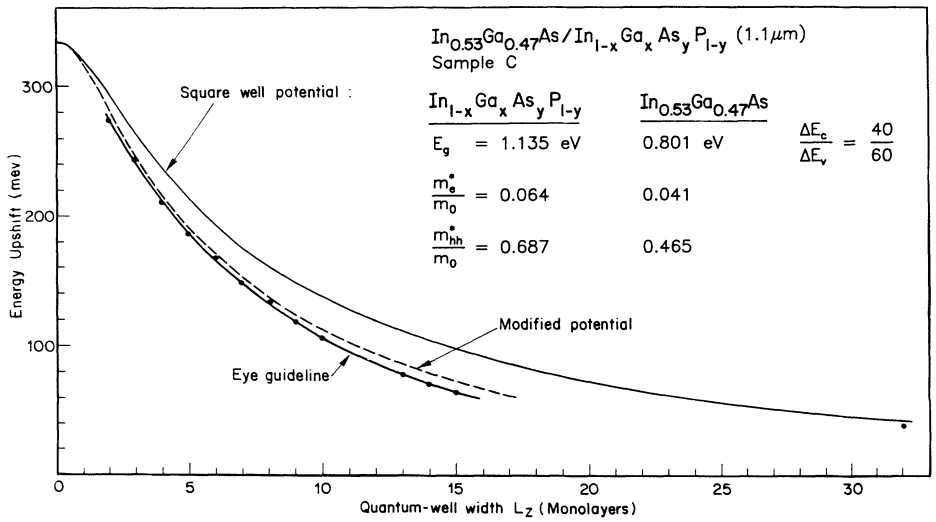

FIG. 8. Spectral upshifts due to particle confinement vs quantum-well widths L_z (in units of 1 ML $= 2.9347$ Å). Experimental data (dots) are from Fig. 3 or Table II. The "square-well potential" curve was calculated using the parameters given in the figure based on a square-shaped potential of the QW's. The "modified potential" curve assumes an exponential excess potential at the bottom of the QW due to a composition swing when starting QW growth (see text).

TABLE II. Wavelengths of the 15 peaks exhibited by sample C at $T=2-4$ K.

Line	Wavelength (μm)
Barrier peak	1.092
2 ML	1.154
3 ML	1.190
4 ML	1.224
5 ML	1.254
6 ML	1.278
7 ML	1.302
8 ML	1.325
9 ML	1.345
10 ML	1.364
13 ML	1.410
14 ML	1.420
15 ML	1.429
94 Å≈32 ML	1.473
Reference	1.547

served for all our $In_{0.53}Ga_{0.47}As/InP$ and $In_{0.53}Ga_{0.47}As/In_{1-x}Ga_xAs_yP_{1-y}$ samples grown on oriented substrates with growth interruption. These considerations motivate us to seek the reason for the discrepancies in a nonsquare form of the well potentials and to discuss below realistic potentials likely to occur in the growth process cycles.

Despite the energetic discrepancies we can make the assignment of PL lines to QW widths L_z shown in Fig. 8. It is based on the facts that for very narrow wells the PL upshifts must approach the total band-gap discontinuity and the particle wave functions are mostly in the barrier material. In this case, mass mixing is negligible, the confinement energies become virtually independent of the form of the localizing potential, and the exciton binding energy takes a three-dimensional small value. Hence, the experimental curve should lie a few milli-electron-volts below the calculated curve. This can only be achieved by our particular assignment in Fig. 8 for sample C. In a similar way, the assignment for sample D in Fig. 3 has been made (see Appendix A). A more direct assignment, in principle preferable to that used here, would consist in the observation of the 1-ML optical transition. In fact, Zachau and Grützmacher[32] in an absorption study proceeded this way studying samples with QW growth times varied in small time intervals of ≈ 0.15 sec from 0 to 2.5 sec. In their absorption spectra they observed islands with widths from 1 to 7 ML's.

In the following, we discuss three possible realistic QW potentials referring to the schematic MOVPE flow diagram in Fig. 1.

A. Intermediate layer model

During the interruption time t_3, after the flux of phosphorus is replaced with arsenic and before the group-III fluxes are initiated, there is a probability that P atoms evaporate and As atoms substitute for P atoms in the surface monolayer so that a monolayer of InAsP is formed. When we attribute bulklike material properties to this monolayer the corresponding band gap would be between 0.43 and 1.425 eV, in the extreme limits of InAs and InP, respectively. This would lead to an intermediate step in the potential as shown in the lower diagram of Fig. 1. An equivalent step could be introduced at the interface between the well and the barrier, giving rise to a monolayer of quaternary $In_{1-x}Ga_xAs_yP_{1-y}$ material. Computations for electrons and holes were done with a potential step 1-ML wide for various negative step potentials (i.e., ML step is lower than the QW bottom), see Appendix B. This procedure lowers the energy eigenvalues as requested by the experiments but the upshift corrections are most significant for very narrow wells, $L_z \approx 1-8$ ML, and tend to decrease rapidly for wider wells contrary to experiment (Fig. 8). This "wrong" shape of the curve was obtained for all choices of the step potential. Therefore we rule out this model as an explanation of the apparent energetic discrepancies.

B. Potential model with compositional transients

In the second model we assume initial lattice mismatch at the onset of QW growth due to perturbed flow rates during the growth interruption cycle. It is well known in MOVPE that small differences between exhaust and reactor line can lead to gas flow perturbations when switching a reactive gas from the first line into the reactor to start growth of the well; this can cause compositional transients. Due to the different vapor pressures of TMGa and TMIn, the H_2 flow into the TMGa source is only small (≈ 8 cm^3/min) for growth of $In_{0.53}Ga_{0.47}As$, and can easily be disturbed; we assume that it takes some time to establish the equilibrium composition of TMGa in the reactor. This makes plausible that at the beginning of the $In_{0.53}Ga_{0.47}As$ well the composition is Ga lean and reaches the final value as in the reference layer only after a certain time. Associated with such compositional transients would be a potential variation $\Delta V(z)$ of the bottom of the QW, equal to the composition-dependent band-gap variation of $In_{0.53}Ga_{0.47}As$. Computations were performed (see Appendix B) taking for $\Delta V(z)$ an exponential with maximum value ΔV_0 and an extension λ of the lattice mismatch or transient-composition variable-potential region. Confinement energies in such modified potentials can be reasonably well fitted to the experimental data for a small range of parameters, ΔV_0 around 30 meV and λ around 100 Å (cf. Fig. 8). Using pertinent $In_{0.53}Ga_{0.47}As$ data[31,39] a variation of the band gap of 30 meV corresponds to approximately 59% indium at the beginning of the QW, instead of 53% indium composition for lattice matching. The experimental point at $L_z=32$ ML in Fig. 8 is underestimated by the fit shown. The reader may be reminded here that we are more discussing trends than quantitatively good fits, the assumed correction potential $\Delta V(z)$ being arbitrarily chosen in its special form. Also, we have not taken into account the (small) strain induced energy shifts necessarily associated with the assumed local mismatch. In summary, it appears that the discrepancies between experiment and theory in Fig. 8 can basically be explained by this model.

A third model worth mentioning includes interfaces with nonvertical potential steps smoothed out due to "memory" effects in the gas flows. Simple approaches would be linearly or exponentially graded potential transitions. We have not considered such a model in detail as evidently narrow well states would be lowered most in energy, with little effect on wider wells contrary to the experimental data.

VI. SCANNING CATHODOLUMINESCENCE RESULTS

Scanning cathodoluminescence was performed on the two samples, *C* and *B*. Cathodoluminescence images were taken by scanning the electron beam over lateral regions of the sample while the recombination light was measured at a fixed wavelength. The spectral resolution was 15 nm. In a second CL mode, the beam excited a fixed spot on the sample, and the luminescence signals were dispersed by scanning the monochromator.

A. Sample *C*

Figure 9 shows CL images of sample *C* of $In_{0.53}Ga_{0.47}As/In_{0.81}Ga_{0.19}As_{0.42}P_{0.58}$. The detection was set to the wavelength 1224 nm corresponding to the 4-ML emission line (left-hand picture) and to 1190 nm corresponding to the 3-ML line (right-hand picture). These two emission lines were chosen as they are the strongest features in the high-energy multiplet of this sample and advance the best spectroscopic resolution due to the energy-versus-wavelength dispersion (cf. Fig. 3). There are bright and dark regions in Fig. 9, of laterally identical shape for the 3- and 4-ML emission light, respectively. One may suppose that at another wavelength the same lateral dark-bright regions emerge. This is indeed demonstrated by the complementary SCL operation mode where we have excited luminescence on a fixed bright and on a fixed "dark" spot in Fig. 9, and have spectroscopically resolved the emitted spectra (Fig. 10). The two spectra are identical, the only difference being the absolute luminescence intensity. The intensity is significantly lower in the "dark" areas yielding much worse signal-to-noise ratio in the lower spectrum of Fig. 10. Similar experiments, with equivalent results, were performed for bright and dark area excitations on various spots as closely together as possible. We conclude from these experiments that the bright regions do not correspond to ML-flat islands and that a resolvable extension of ML-flat islands must be confined to a lateral scale smaller than the present one given by the spatial resolution of the CL system, of $\lesssim 2\ \mu$m (see Sec. II). It is clear from the data that the dark-bright contrast in Fig. 9 originates from lateral quantum efficiency differences in the sample. These may be due to nonradiative defects which trap electrons and/or holes and hence, quench luminescence to the same extent for *all* emission lines.

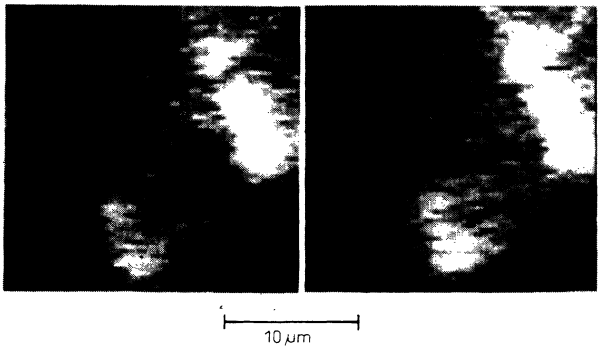

FIG. 9. Scanning cathodoluminescence (SCL) monochromatic images of sample *C* of $In_{0.53}Ga_{0.47}As/In_{0.81}Ga_{0.19}As_{0.42}P_{0.58}$. Left-hand side: light detection on the 4-ML peak ($\lambda = 1.224\ \mu$m); right-hand side: light detection on the 3-ML peak ($\lambda = 1.190\ \mu$m), cf. Fig. 3.

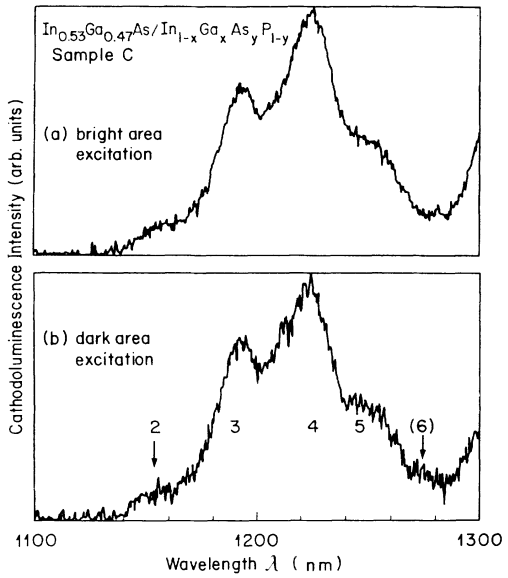

FIG. 10 "Spot excitation spectra" in scanning cathodoluminescence experiments on sample *C* of $In_{0.53}Ga_{0.47}As/In_{0.81}Ga_{0.19}As_{0.42}P_{0.58}$. (a) and (b) refer to the dark-bright images of Fig. 9. Due to the weak light intensities from the "dark" regions the signal-to-noise ratio in (b) is significantly worse than in (a). The numbers in (b) are the thicknesses L_z of the emitting islands in monolayers as in Fig. 3.

It is interesting to compare these results with SCL data of others which were recently reported for $GaAs/Al_{1-x}Ga_xAs$ QW's. Bimberg *et al.*[8,9] studied a triplet PL structure ascribed to ML-flat islands of 18-, 19-, and 20-ML widths, respectively, of MBE grown sample by CL imaging. On a lateral scale comparable in size to ours they found for each of the triplet lines bright-dark lateral patterns *different* for the three wavelengths, and concluded that the bright areas represented the lateral extensions of 18-, 19-, or 20-ML-wide islands, respectively. In a more recent paper, Christen, Grundmann, and Bimberg[40] studied the same samples with an improved SCL technique and could show that the lateral regions giving rise to the three emission lines are essentially complementary and cover completely macroscopic sample regions. Wada *et al.*[41] in their SCL study of MBE grown $GaAs/Al_{0.5}Ga_{0.5}As$ QW's observed in monochromatic CL images dark-bright stripe patterns with periodicity in

the 0.6-μm range. They associated the patterns with "clustered terrace" formation in the heterointerface basically due to the inadvertent residual offset angle of $\approx 0.2°$ for "exactly" oriented substrates. Stützler *et al.*,[10] in MOVPE grown GaAs/$Al_{0.5}Ga_{0.5}As$ QW's, observed in PL spectra a doublet splitting of a high-energy emission line from a nominally 18-Å narrow QW, which they ascribed to extended ML-flat islands in this QW. Concomitant CL images, with light detection on the two doublet peaks, showed irregularly shaped bright-dark lateral regions of ~ 1 μm size on average, with partially complementary brightness. None of these different features in the works cited is observed in our work when the monochromator is set on intensity maxima of various multiplet lines.

B. Sample *B*

A second CL experiment was performed on sample *B* of $In_{0.53}Ga_{0.47}As/InP$ where, similar to sample *C* of $In_{0.53}Ga_{0.47}As/In_{0.81}Ga_{0.19}As_{0.42}P_{0.58}$ a multiplet PL spectrum indicates the formation of islands with 2-, 3-, and 4-ML widths (cf. Fig. 2). In this sample, the 3-ML peak is dominant over all other peaks thus enabling the following experiment. Instead of detecting luminescence on the peaks of two different ML lines for CL images, we compare two CL images taken with light detection on the positive and negative flanks of the 3-ML line at approximately half maximum intensity and with a spectral resolution of 15 nm (Fig. 11). In this case we do find complementary dark-bright lateral regions at these two detection wavelengths. The complementary features are extremely well developed on the right-hand side of the diagrams in Fig. 11, e.g., in the middle and in the lower corner. Depending on the adjustment of the contrast ratio in plotting the diagrams complementary dark-bright structures can be recognized over almost the whole area depicted in Fig. 11. In the spot excitation mode, we have excited fixed spots on the sample close to the dark-bright transitions and have spectroscopically resolved the CL. Results were obtained as shown in Fig. 12 as an example.

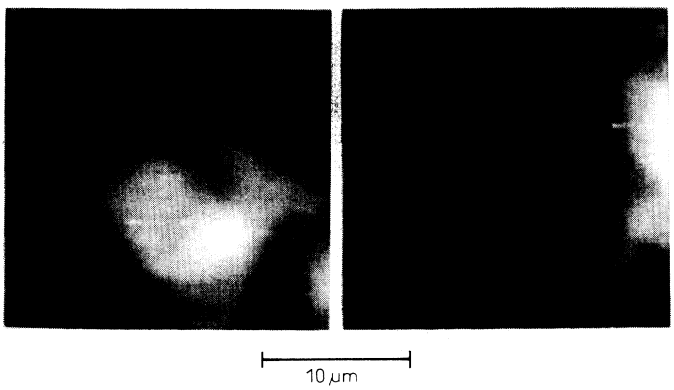

FIG. 11. Scanning cathodoluminescence (SCL) monochromatic images of sample *B* of $In_{0.53}Ga_{0.47}As/InP$. Left-hand side: light detection on the left shoulder of the 3-ML peak ($\lambda = 1.001$ μm); right-hand side: light detection on the right shoulder of the 3-ML peak ($\lambda = 1.022$ μm), cf. Fig. 2.

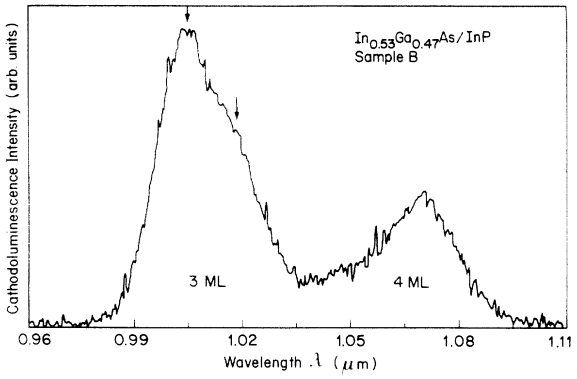

FIG. 12. "Spot excitation spectra" in scanning cathodoluminescence experiments on sample *B* of $In_{0.53}Ga_{0.47}As/InP$. A spot at a dark-bright transition in Fig. 11 was excited by the electron beam. The spectrum shows fine splitting of the 3-ML peak (indicated by arrows) and a splitting/shift effect also of the 4-ML peak (see text). The halfwidth of the 3-ML structure is 28 nm (33.6 meV), as compared to 29.5 nm (36 meV) of the 3-ML line in Fig. 2; both fine structures lie essentially within the shapes of the 3- and 4-ML lines, respectively, of Fig. 2.

The 3-ML line splits into a doublet and concomitantly, the 4-ML line also seems to split or, at least, to shift its major component. [In Fig. 12, e.g., the spacing between the 3- and 4-ML lines from Fig. 2 is reproduced between the peak of the 4-ML line and the side component (lower arrow) of the 3-ML line. This indicates that the 4-ML line is split into a doublet as is the 3-ML line.] It is important to note that the fine structure of the lines in Fig. 12 lies essentially within the shapes of the 3- and 4-ML lines of Fig. 2 obtained in photoluminescence. This shows that the SCL mode chosen selects out special portions from the full, spatially unresolved lines that are associated with the complementary luminescing areas in Fig. 11. Similar complementary dark-bright structures over complex-shaped regions as in Fig. 11 have been observed when different sample spots were monitored.

An explanation of these data is straightforward. All bright areas in Fig. 11 emit part of the same broad luminescence line but their lateral structures are associated either with the low-energy side of the line (left-hand CL image) or with the high-energy side of the line (right-hand CL image). Hence, the effect causing the lateral image structure is also responsible for the enhanced linewidths typical of the growth-interruption cycle defined earlier. To be specific, for sample *B* grown with $t_3 = 2s$ interruption time the halfwidth (FWHM) is ≈ 36 meV whereas sample *A*2 with $t_3 = 0.5$ sec (Fig. 2) exhibits less than half of this value. As the lines broaden on a scale below ML spacings (58 meV between the 3- and 4-ML lines in Fig. 2) the only effect that could be responsible for these different emission energies within a line is a perturbation of the QW potentials fluctuating in the different island regions. It is more than natural to assume that such QW potential fluctuations are the same ones which were discussed earlier and were ascribed to compositional mismatch when growth of a new QW is started.

The objection that such lateral fluctuations of the excess potential $\Delta V(z)$ should be continuous, whereas in Fig. 11 we observe, ideally, "digital" structure in the bright-dark contrast, can be refuted: in monitoring the contrast at the two positions on each side of the peak (at about 50% maximum intensity) with approximately nonoverlapping but almost line-covering resolution we average out more detailed bright-dark structure and cast the total contrast information into the two detection "classes." Hence, we expect to see more complex-shaped bright-dark regions in Fig. 11 for better spectroscopic resolution. However, this cannot be achieved at present.

To summarize this section, the grossest scale in our lateral investigations is realized by a laser beam focused to an excitation spot of ~ 100 μm. On this scale, no spatial variations of the PL spectra are observed; hence, any spot monitored must contain the same distribution of QW changes and fluctuations, such as island sizes and QW potentials. The finest scale is represented by the extended ML-flat islands within a given QW, with a perpendicular scale of 1 ML=2.9347 Å. The lateral island size must be larger than the sum of exciton diameter and low-temperature diffusion length but smaller than the effective lateral resolution of the SCL, approximately between 0.3 and 2 μm. Within the sampled area of the electron beam, QW islands of individual ML widths are contained in an "identical" distribution. The complementary regions in Fig. 11 appear on a scale from ≈ 1 μm up. These regions include islands with specific potential fluctuations out of a whole manifold $\delta(\Delta V(z))$ given by flow inhomogeneities; the observed potential fluctuations are—by means of the limited spectroscopic resolution in SCL—in two classes with, on the average, higher or lower values of the excess mismatch potential $\Delta V(z)$, respectively.

VII. CONCLUSION

Low-pressure MOVPE growth of lattice-matched $In_{0.53}Ga_{0.47}As/InP$ and $In_{0.53}Ga_{0.47}As/In_{1-x}Ga_xAs_yP_{1-y}$ quantum wells was studied on oriented and misoriented (100) substrates with different growth-interruption cycles. Quantum wells have been obtained which split up into four or five luminescent island regions with islands widths L_z differing by monolayer thicknesses. One sample containing nominally four QW's with appropriately chosen widths showed overlapping PL line spectra from 11 islands; these could be associated with a coherent sequence of island widths from 2 to 15 monolayers. This sample and similar others providing the same material quality in all QW's are excellently suited to study L_z-dependent optical properties. Exciton transfer is not observed between the islands at low temperature but sets in at higher temperatures in the range of 90 K. When the islands are decoupled at low temperatures, the exciton lifetimes as a function of L_z form a rather smooth curve with a minimum value $\tau \approx 1.5$ ns at $L_z \approx 20$–30 Å. The experimental curve can satisfactorily be fitted by a simple model expressing τ in terms of the vertical electron-hole overlap and the vertical exciton extension. The availability of 14 coherent confinement energies allows for a comparison with the standard theory of energy states in square wells. It is shown that the assumption of square wells is inconsistent with the data. Realistic potentials are discussed. The data can be explained by a model assuming that, due to flow inhomogeneities by the growth interruption, each well is grown with an initial mismatch over the first 100 Å before lattice matching is achieved. Scanning cathodoluminescence measurements were performed on two samples. In one of the samples, of $In_{0.53}Ga_{0.47}As/InP$, we observe complementary dark and bright areas associated with PL detection on the lower- or higher-energy side of the same island PL line. It is argued that the local mismatch along the first 100 Å of a QW is nonuniform across a sample (parallel to the QW), thus causing additional lateral fluctuations of the associated QW potential.

ACKNOWLEDGMENTS

The authors thank T. Forster of IBM Rüschlikon for essential help in performing the SCL experiments. The work of one of us (R.S.) was done in part at the University of Ulm.

APPENDIX A

The parameter values used and their influence on the confinement energies in square wells are discussed. The full curve in Fig. 8 was calculated using Bastard's boundary conditions[37] and the parameter set given in the figure. The effective band gaps of $In_{0.53}Ga_{0.47}As$ and $In_{1-x}Ga_xAs_yP_{1-y}$ were experimentally obtained from the recombination lines of the reference layer and the barrier, respectively (see Fig. 3). Therefore, the total band-gap discontinuity is empirically determined. The total offset was partitioned among conduction and valence bands as $\Delta E_c:\Delta E_v = 40:60$ consistent with the finding of Forrest *et al.*[42] who determined $\Delta E_c = 0.39\,\Delta E_g$ for the complete range of compositions in the $In_{1-x}Ga_xAs_yP_{1-y}/InP$ system from InP to $In_{0.53}Ga_{0.47}As$, and with Zachau *et al.*,[43] who found $\Delta E_c = 0.36\,\Delta E_g$ for selected values of the composition close to the $In_{0.53}Ga_{0.47}As$ limit. Mass values are from Refs. 31 and 39, where for $In_{1-x}Ga_xAs_yP_{1-y}InP$ ($y \approx 0.42$) with $E_g \approx 1.135$ eV a linear interpolation was applied: $m_e^* = 0.080 - 0.039y$ and $m_{hh}^* = 0.85 - 0.385y$. The influence of the masses on the first QW subband $n=1$ is only small. This can be visualized by graphic representation of the corresponding secular equation and has been discussed by Nelson, Miller, and Kleinman.[44] The energy dependence of the masses, due to the coupling of electrons, light holes, and split-off holes, was computed in a Kane three-band $\mathbf{k}\cdot\mathbf{p}$ perturbation calculation[45,46] and yields *larger* upshifts for the $n=1$ subbands than without coupling. This positive upshift correction is ≈ 4 meV at maximum for 50–80-Å wide QW's. (In contrast, all excited states are lowered, to a much larger extent.)

The experimental energies include the exciton binding energy which has to be added to the data for a comparison with computations. Theory yields L_z-dependent

binding energies E_x of excitons in QW's.[47] In the particular case of lattice-matched $In_{1-x}Ga_xAs/InP$ quantum wells, Lin *et al.*[48] measured exciton binding energies by thermally modulated PL, and found a maximum value of $E_x = 18$ meV for $L_z = 12$ Å, with sharp drops to values of around 8 meV for smaller and larger widths. Therefore, when dealing with narrow wells of ≈ 6–10-Å thickness a value of $E_x \approx 10$ meV may represent a fairly good approach. This value was also applied as a representative value in recent PLE studies of excited excitonic transitions in lattice-matched $In_{1-x}Ga_xAs/InP$ QW's.[49] With a proper account of E_x, the experimental points in Fig. 8 should be roughly 10 meV below computed confinement energies for the narrowest wells.

For sample *D*, a totally equivalent situation to example *C* is found when energy upshifts are compared to computed values. Here, the barrier material $In_{1-x}Ga_xAs_yP_{1-y}$ has a slightly different composition, $y \approx 0.38$, as obtained from the band-edge position $E_g \approx 1.158$ eV (Fig. 3). We have taken appropriate masses—as given by the above-mentioned *y*-dependent interpolation expressions—to calculate an energy-vs-QW-width curve, and have cross-related growth times and PL peak positions in Fig. 3 of samples *C* and *D*. This leads us to the line assignment given in Fig. 3.

Finally, the general problem arises whether it is physical to apply simple square-well potentials to quantum wells as narrow as a few monolayers, without account of microscopic features on this scale. We cannot answer this question in principle as it stands but we refer to the work of Morais *et al.*[23] on samples grown by vapor levitation epitaxy where excellent agreement between the simple standard theory and experimental data was found even for QW's two monolayers wide. This gives us confidence that our conclusions from a comparison of experiment and standard theory are physically meaningful.

APPENDIX B

The calculation of eigenstate energies in a square-well potential with a step were performed using the secular equation

$$\tan(\alpha l)\{(1-\eta^2)+\eta(\gamma/\alpha+\alpha/\gamma)\tan[\gamma(L-l)]\} -2\eta-(\eta^2\alpha/\gamma-\gamma/\alpha)\tan[\gamma(L-l)]=0 , \quad \text{(B1)}$$

where

$$\alpha=[(2m_w/\hbar^2)E]^{1/2},\ \beta=[(2m_b/\hbar^2)(V_0-E)]^{1/2} ,$$
$$\gamma=[(2m_w/\hbar^2)(E-V_1)]^{1/2},\ \eta=(\beta m_w)/(\alpha m_b) .$$

The equation was derived from basic quantum mechanics. The barrier mass is m_b, the QW mass is m_w, and the widths of the step and the whole QW are $(L-l)$ and L, respectively. V_0 denotes the barrier potential and V_1 the step potential, and the QW bottom is at $E=0$. Equation (B1) is consistent with analogous expressions obtained in a different form from theoretical calculations of others.[50] When the step is positive (between the top and the bottom of the QW) the eigenvalues of electrons and heavy holes in the well are lifted and vice versa.

The calculation of eigenstate energies in the potential swing model assuming initial local lattice mismatch was based on the simple exponential (although somewhat arbitrary) form of the excess potential,

$$\Delta V(z) = -\Delta V_0 \exp(-z/\lambda) , \quad \text{(B2)}$$

where the beginning of the QW is chosen at $z=0$ and λ defines the extension of the extra potential (or the lattice mismatch) in the growth direction z. For electrons, the potential is sketched in Fig. 1 (lower diagram); the unperturbed potential of the QW bottom is at $E=0$ and the share of the electrons in the total value of V_0 is given by the conduction- to valence-band offsets. The hole extra potential is taken accordingly. The excess potential is negative when the QW composition is Ga-poor (In-rich) at the beginning. As long as the maximum excess potentials for electrons and holes, for $z=0$, are much smaller than the unperturbed QW square potentials, the effect of the excess potentials on the confinement energies may be approximated by first-order perturbation theory,

$$\Delta E = \frac{\int \psi^* \Delta V(z) \psi \, dz}{\int \psi^* \psi dz} , \quad \text{(B3)}$$

with wave functions for electrons and holes normalized in the whole QW and barrier range. Computations were made for electrons and holes by varying the extension parameter λ and the maximum excess potential ΔV_0 to yield corrected QW confinement energies; the sum of the corrected electron and hole energies yields the corresponding upshift. As expected, the modified upshifts are small for very narrow wells (as the eigenstates are close to the top of the wells, nearly insensitive to the excess potential at the QW bottom) and for very wide wells $L_z \gg \lambda$ (as the excess potential has influence only in an increasingly smaller portion of the well). In the intermediate L_z range, there is not much space for varying λ and ΔV_0 in order to obtain reasonable fits to the experimental points. An example is given in Fig. 8 for the fit parameters $\Delta V_0 = 30$ meV and $\lambda = 100$ Å.

---

*Permanent address: Department of Semiconductor Physics, University of Ulm, P.B. 4066, D-7900 Ulm, Germany.

†Permanent address: Department of Solid State Physics, University of Lund, Box 118, S-221 00 Lund, Sweden.

[1]T. Hayakawa, T. Suyama, K. Takahashi, M. Kondo, S. Yamamoto, S. Yano, and T. Hijikata, Appl. Phys. Lett. **47**, 952 (1985).

[2]T. Hayakawa, T. Suyama, K. Takahashi, M. Kondo, S. Yamamoto, S. Yano, and T. Hijikata, Surf. Sci. **174**, 76 (1986).

[3]T. Fukunaga, K. L. I. Kobayashi, and H. Nakashima, Surf. Sci. **174**, 71 (1986).

[4]F. Voillot, A. Madhukar, J. Y. Kim, P. Chen, N. M. Cho, W. C. Tang, and P. G. Newman, Appl. Phys. Lett. **48**, 1009 (1986).

[5]D. Bimberg, D. Mars, J. N. Miller, R. Bauer, and D. Oertel,

Sci. Technol. B **4**, 1014 (1986).
[6]B. A. Wilson, R. C. Miller, S. K. Sputz, T. D. Harris, R. Sauer, M. G. Lamont, C. W. Tu, and R. F. Kopf, in *13th International Symposium on GaAs and Related Compounds, Las Vegas, 1986,* edited by W. T. Lindley, IOP Conf. Proc. No. 83 (Institute of Physics and Physical Society, London, 1986), p. 215.
[7]R. C. Miller, C. W. Tu, S. K. Sputz, and R. F. Kopf, Appl. Phys. Lett. **49**, 1245 (1986).
[8]D. Bimberg, J. Christen, T. Fukunaga, H. Nakashima, D. E. Mars, and J. N. Miller, J. Vac. Sci. Technol. B **5**, 1191 (1987).
[9]D. Bimberg, J. Christen, T. Fukunaga, H. Nakashima, D. E. Mars, and J. N. Miller, Superlatt. Microstruct. **4**, 257 (1988).
[10]F. J. Stützler, S. Fujieda, M. Mizuta, and K. Ishida, Appl. Phys. Lett. **53**, 1923 (1988).
[11]H. Sakaki, M. Tanaka, and J. Yoshino, Jpn. J. Appl. Phys. **24**, L417 (1985).
[12]M. Tanaka, H. Sakaki, J. Yoshino, and T. Furuta, Surf. Sci. **174**, 65 (1986).
[13]T. Y. Wang, K. L. Fry, A. Persson, E. H. Reihlen, and G. B. Stringfellow, J. Appl. Phys. **63**, 2674 (1988).
[14]M. Irikawa, I. J. Murgatroyd, T. Ijichi, N. Matsumoto, A. Nakai, and S. Kashiwa, J. Cryst. Growth **93**, 370 (1988).
[15]M. Kondo, S. Yamazaki, M. Sugawara, H. Okuda, K. Kato, and K. Nakajima, J. Cryst. Growth **93**, 376 (1988).
[16]F.-Y. Juang, P. K. Bhattacharya, and J. Singh, Appl. Phys. Lett. **48**, 290 (1986).
[17]L. Goldstein, Y. Horikoshi, S. Tarucha, and H. Okamoto, Jpn. J. Appl. Phys. **22**, 1489 (1983).
[18]B. Deveaud, J. Y. Emery, A. Chomette, B. Lambert, and M. Baudet, Appl. Phys. Lett. **45**, 1078 (1984).
[19]D. C. Reynolds, K. K. Bajaj, C. W. Litton, P. W. Yu, J. Singh, W. T. Masselink, R. Fischer, and H. Morkoç, Appl. Phys. Lett. **46**, 51 (1985).
[20]B. Devaud, A. Regreny, J. Y. Emery, and A. Chomette, J. Appl. Phys. **59**, 1633 (1986).
[21]P. J. A. Thijs, E. A. Montie, H. W. van Kesteren, and G. W. 't Hooft, Appl. Phys. Lett. **53**, 971 (1988).
[22]P. J. A. Thijs, T. van Dongen, P. I. Kuindersma, J. J. M. Binsma, L. F. Tiemeyer, and J. M. Lagemaat, J. Cryst. Growth **93**, 863 (1988).
[23]P. C. Morais, H. M. Cox, P. L. Bastos, D. M. Hwang, J. M. Worlock, E. Yablonovitch, and R. E. Nahory, Appl. Phys. Lett. **54**, 442 (1989).
[24]In adopting the naive model of extended flat islands in a QW we are aware of inconsistencies between optical measurements (PL, PLE, absorption) and high-resolution electron microscopy ("chemical lattice imaging") on the roughness of QW interfaces that have recently been pointed out in C. A. Warwick, W. Y. Jan, A. Ourmazd, and T. D. Harris, Appl. Phys. Lett. **56**, 2666 (1990). While, basically, in the present paper we remain with the flat island model, our later discussion of perpendicular and lateral potential fluctuations and distributions as deduced from our optical techniques approaches ideas advanced by Warwick *et al.* on spatial roughness distribution.
[25]B. G. Yacobi and D. B. Holt, *Cathodoluminescence Microscopy of Inorganic Solids* (Plenum, New York, 1990). See also T. E. Everhart and P. H. Hoff, J. Appl. Phys. **42**, 5837 (1971).
[26]H. Hillmer, Ph.D. thesis, University of Stuttgart, 1989.
[27]H. Kakibayashi and F. Nagata, Jpn. J. Appl. Phys. **25**, 1644 (1986).
[28]P. A. Buffat, J. D. Ganière, and P. A. Stadelmann, in *Evaluation of Semiconductor Materials by Electron Microscopy,* edited by David Cherns (Plenum, New York, 1990), p. 319.
[29]R. Spycher, P. A. Buffat, P. A. Stadelmann, P. Roentgen, W. Heuberger, and V. Graf, in *Microscopy of Semiconducting Materials 1989,* Proceedings of the Royal Microscopical Society Conference No. 6, edited by A. G. Cullis and J. L. Hutchinson, IOP Conf. Proc. No. 100 (Institute of Physics and Physical Society, London, 1989), p. 299.
[30]R. Spycher, P. A. Stadelmann, and P. A. Buffat, in *Epitaxial Heterostructures,* edited by D. W. Shaw *et al.*, MRS Symposia Proceedings No. 198 (Materials Research Society, Pittsburgh, 1990), p. 135.
[31]*GaInAsP Alloy Semiconductors,* edited by T. P. Pearsall (Wiley, New York, 1982).
[32]M. Zachau and D. Grützmacher, Appl. Phys. Lett. **56**, 632 (1990).
[33]U. Cebulla, G. Bacher, G. Mayer, A. Forchel, W. T. Tsang, and M. Razeghi, Superlatt. Microstruct. **5**, 227 (1989).
[34]U. Cebulla, G. Bacher, A. Forchel, G. Mayer, and W. T. Tsang, Phys. Rev. B **39**, 6257 (1989).
[35]J. Feldmann, G. Peter, E. O. Göbel, P. Dawson, K. Moore, C. Foxon, and R. J. Elliott, Phys. Rev. Lett. **59**, 2337 (1987); **60**, 243(E) (1988).
[36]In Refs. 33 and 34 the parameter M appearing in the theory of Ref. 35 was cited as the "reduced mass" of the exciton. This is incorrect.
[37]G. Bastard, Phys. Rev. B **24**, 5693 (1981).
[38]M. Engel, R. K. Bauer, D. Bimberg, D. Grützmacher, and H. Jürgensen, J. Cryst. Growth **93**, 359 (1988).
[39]*Zahlenwerte and Funktionen aus Naturwissenschaft und Technik,* edited by O. Madelung, M. Schulz, and H. Weiss, Landolt-Börnstein, New Series, Vol. 17a (Springer, Berlin, 1982).
[40]J. Christen, M. Grundmann, and D. Bimberg, Appl. Surf. Sci. **41/42**, 329 (1989).
[41]K. Wada, A. Kozen, Y. Hasumi, and J. Temmyo, Appl. Phys. Lett. **54**, 436 (1989).
[42]S. R. Forrest, P. H. Schmidt, R. B. Wilson, and M. L. Kaplan, Appl. Phys. Lett. **45**, 1199 (1984).
[43]M. Zachau, P. Helgesen, A. Kux, F. Koch, D. Grützmacher, R. Meyer, H. Jürgensen, and P. Balk, Superlatt. Microstruct. **5**, 19 (1989).
[44]D. F. Nelson, R. C. Miller, and D. A. Kleinman, Phys. Rev. B **35**, 7770 (1987).
[45]E. O. Kane, J. Phys. Chem. Solids **1**, 249 (1957).
[46]M. F. H. Schuurmans and G. W. 't Hooft, Phys. Rev. B **31**, 8041 (1985).
[47]A comprehensive listing of theoretical work on exciton binding energies in QW's is given in U. Ekenberg and M. Altarelli, Phys. Rev. B **35**, 7585 (1987).
[48]Z. H. Lin, T. Y. Wang, G. B. Stringfellow, and P. C. Taylor, Appl. Phys. Lett. **52**, 1590 (1988).
[49]D. Gershoni, H. Temkin, and M. B. Panish, Phys. Rev. B **38**, 7870 (1988).
[50]V. K. Tripathi and P. K. Bhattacharya, Superlatt. Microstruct. **1**, 73 (1985).

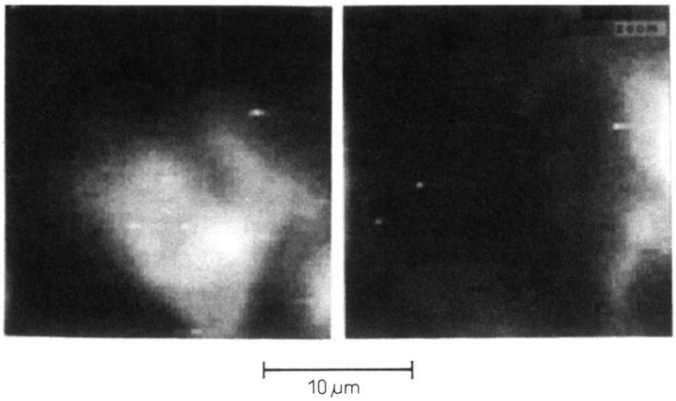

FIG. 11. Scanning cathodoluminescence (SCL) monochromatic images of sample *B* of $In_{0.53}Ga_{0.47}As/InP$. Left-hand side: light detection on the left shoulder of the 3-ML peak ($\lambda = 1.001$ μm); right-hand side: light detection on the right shoulder of the 3-ML peak ($\lambda = 1.022$ μm), cf. Fig. 2.

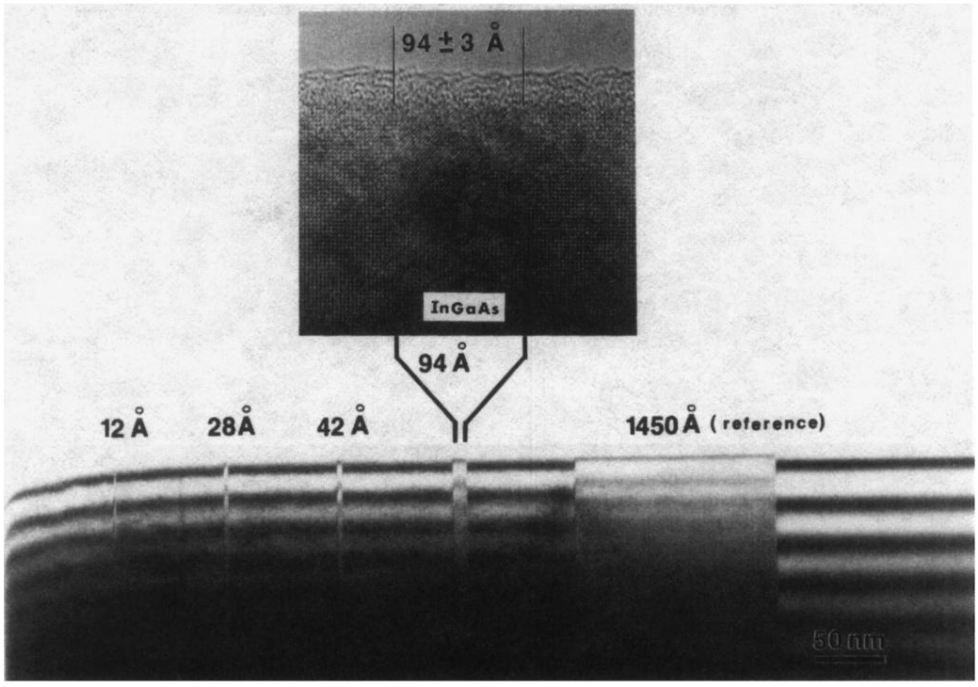

FIG. 4. Transmission electron microscopic picture of part of sample C ($In_{0.53}Ga_{0.47}As/In_{0.81}Ga_{0.19}As_{0.42}P_{0.58}$) showing the four QW's and the reference layer. The high-resolution picture on top yields the thickness of the widest QW, $L_z=(94\pm3)$ Å, and is used to calibrate the bright field image on the bottom. The widths obtained for the three remaining QW's are $L_z=42$, 28, and ≈ 12 Å. The reference layer of $In_{0.53}Ga_{0.47}As$ is 1450-Å thick.

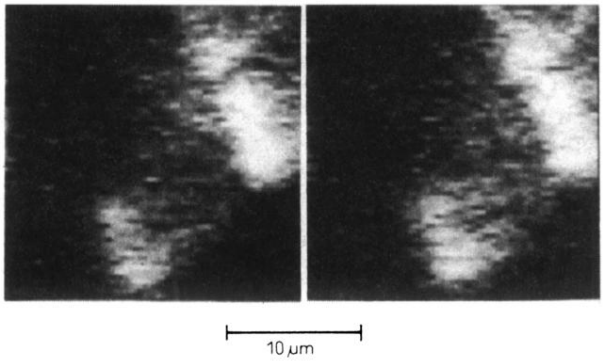

FIG. 9. Scanning cathodoluminescence (SCL) monochromatic images of sample *C* of $In_{0.53}Ga_{0.47}As/In_{0.81}Ga_{0.19}As_{0.42}P_{0.58}$. Left-hand side: light detection on the 4-ML peak ($\lambda = 1.224$ μm); right-hand side: light detection on the 3-ML peak ($\lambda = 1.190$ μm), cf. Fig. 3.